This is the peer reviewd version of the followng article:

Raman scattering with infrared excitation resonant with the MoSe2 indirect band gap / Sotgiu, S.; Venanzi, T.; Macheda, F.; Stellino, E.; Ortolani, M.; Postorino, P.; Baldassarre, L.. - In: PHYSICAL REVIEW. B. - ISSN 2469-9950. - 106:8(2022), pp. N/A-N/A. [10.1103/PhysRevB.106.085204]

Terms of use:

The terms and conditions for the reuse of this version of the manuscript are specified in the publishing policy. For all terms of use and more information see the publisher's website.

17/05/2026 06:44

(Article begins on next page)

arXiv:2208.02505v1 [cond-mat.mtrl-sci] 4 Aug 2022

Raman Scattering with infrared excitation resonant with $MoSe_2$ indirect band gap

Simone Sotgiu,[1,*] Tommaso Venanzi,[1] Francesco Macheda,[2] Elena Stellino,[3] Michele Ortolani,[1] Paolo Postorino,[1] and Leonetta Baldassarre[1,†]

[1]*Department of Physics, Sapienza University of Rome, Piazzale Aldo Moro 5, 00185 Roma, Italy*
[2]*Istituto Italiano di Tecnologia, Graphene Labs, Via Morego 30, I-16163 Genova, Italy*
[3]*Department of Physics and Geology, University of Perugia, via Alessandro Pascoli, Perugia, Italy*

(Dated: August 5, 2022)

Resonance Raman scattering, which probes electrons, phonons and their interplay in crystals, is extensively used in two-dimensional materials. Here we investigate Raman modes in $MoSe_2$ at different laser excitation energies from 2.33 eV down to the near infrared 1.16 eV. The Raman spectrum at 1.16 eV excitation energy shows that the intensity of high-order modes is strongly enhanced if compared to the first-order phonon modes intensity due to resonance effects with the $MoSe_2$ indirect band gap. By comparing the experimental results with the two-phonon density of states calculated with density functional theory, we show that the high-order modes originate mostly from two-phonon modes with opposite momenta. In particular, we identify the momenta of the phonon modes that couple strongly with the electrons to produce the resonance process at 1.16 eV, while we verify that at 2.33 eV the two-phonon modes lineshape compares well with the two-phonon density of state calculated over the entire Brillouin Zone. We also show that, by lowering the crystal temperature, we actively suppress the intensity of the resonant two-phonon modes and we interpret this as the result of the increase of the indirect band gap at low temperature that moves our excitation energy out of the resonance condition.

Raman scattering is a widely used spectroscopic technique to study the vibrational and electronic excitations in solids. When the incoming laser energy matches a real electronic transition, in a so-called resonance effect, an enhancement of the Raman cross-section occurs with respect to non-resonant processes, leading to a higher visibility of otherwise hidden modes and of high-order Raman modes, providing information on electronic transitions, phonon-dispersion and electron-phonon interaction [1–5].

Resonance Raman spectroscopy has been extensively employed to study graphene and other two-dimensional materials as it provides information on their vibrational properties [6–9], on the presence of defects [10, 11], and it is used to identify different stacking orders [12] and for growth quality check [13]. Among the vast class of two dimensional materials, the semiconductor compounds, such as the transition metal dichalcogenides (TMDs) MX_2 with M=Mo,W and X=S,Se,Te, have attracted a particular interest because of their potential applications in opto-electronic devices. The layered crystal structure, which leads to an extreme surface-to-volume ratio in the single layers, makes these materials one of the most promising candidates for the development of flexible and ultraflat opto-electronic devices [14–18].

$MoSe_2$ was shown to be attractive for several applications such as electrochemical energy storage, due to its particular chemical properties and its good conductivity [19], and as near-infrared photodetectors [20] thanks to its thickness dependent band-gap width (indirect band gap of 1.14 eV for $MoSe_2$ bulk and 1.6 eV direct band gap for monolayers) [16, 21], and its high optical absorption in the near-infrared region [22]. A deep understanding of the scattering channels, e.g. electron-phonon scattering and of the related charge carrier transport properties [23–25] is mandatory for the implementation of TMDs in any opto-electronic device. To this end, resonance Raman scattering provides a unique possibility to address the scattering processes in $MoSe_2$ using several excitation energies, from visible to near UV [26–29]. However, to the best of our knowledge, the lowest excitation energy used was 1.58 eV, hence no Raman scattering has been reported so far with incoming photon resonant with the indirect band gap of $MoSe_2$, meaning that no study of the interaction of electrons at the bottom of the conduction band with the phonons has been performed up to now.

In this work, we present a resonance Raman scattering study of $MoSe_2$ crystals measured with an incoming photon energy of 2.33 and 1.96 eV and 1.16 eV that matches the indirect band-gap transition of $MoSe_2$. For the latter photon excitation energy we observe a great enhancement of the scattering intensity of high-order processes with respect to first-order modes. By comparing the Raman spectra with the two-phonon density of states (2ph-DOS) calculated by Density Functional Theory (DFT), we associate these peaks with two-phonon resonant Raman processes involving the electronic transition at the indirect band gap of the crystal. Our results deepen the understanding of Raman scattering in $MoSe_2$, indicating that phonon modes with momenta comparable to that connecting the indirect band-gap points in the Brillouin zone are strongly coupled to electrons. Our results, moreover, demonstrate that the near-infrared excitation radiation can be used as a powerful tool to study small-gap semiconductors obtaining relevant information on the material properties. [30].

I. METHODS

Raman spectra at 1.16 eV excitation energy are collected with a Fourier-transform interferometer (Bruker MultiRAM), equipped with a Nd:YAG laser and a nitrogen-cooled Germanium detector (spectral range 5900-11700 cm^{-1}), and con-

* Corresponding author: simone.sotgiu@uniroma1.it
† Corresponding author: leonetta.baldassarre@uniroma1.it

nected via optical fibers to an optical microscope. The spectra at room temperature are obtained with a 100x objective (Numerical Aperture 0.85), spectral resolution of 1 cm^{-1} and a power density around 2.5 $mW/\mu m^2$. The temperature-dependent measurements are performed with a He-flow cryostat and a 4x objective. We set 2 cm^{-1} resolution and 0.02 $mW/\mu m^2$ power density. The spectra at 2.33 eV and 1.96 eV excitation energy are measured with a Horiba HR Evolution microspectrometer equiped with a 100x objective coupled to a Silicon CCD camera. We measure with 0.6 cm^{-1} spectral resolution and power density of 5 and 0.5 $mW/\mu m^2$ for 2.33 and 1.96 eV respectively. $MoSe_2$ single crystals are purchased from *HQ Graphene*. The absorbance spectrum is obtained from a transmission experiment using Bruker FT-IR spectrometer. For DFT calculations we used a GGA-PBE functional with semi-empirical Grimme-D3 van der Waals corrections [31] to optimize the geometry of the structure, employing a energy cutoff of 125 Ry and a **k**-point grid of dimensions $15\times15\times3$. The optimization leads to a lattice parameter of a = 6.266 Bohr and an interlayer distance of 24.665 Bohr, in accordance with [32]. The position of the electronic band gap is dependent on the interlayer distance, which is incorrectly overestimated if the van der Waals corrections are not taken in account. The 2ph-DOS—namely, $DOS_{2\omega}(\varepsilon)=\sum_{\mathbf{q}\mu\nu}\delta(\varepsilon-\omega_{\mathbf{q}\nu}-\omega_{\mathbf{q}\mu})$, $\omega_{\mathbf{q}\mu,\nu}$ being the phonon frequency—is obtained computing the phonons using Density Functional Perturbation Theory [33] on a **q**-points grid of dimensions $6\times6\times2$, which is then interpolated on a $768\times768\times1$ grid to evaluate the sums in the expression for $D_{2\omega}(\varepsilon)$. All the calculations have been performed using the QUANTUM ESPRESSO suite [34].

II. RESULTS AND DISCUSSION

First of all we determine experimentally the energy of the indirect band gap at room temperature in order to compare it with our laser lines. We measure both the photoluminescence (PL) and the absorbance spectrum and use a Tauc procedure to extract the band-gap width [35, 36] (see Figure 1). The discrepancy between the value obtained from the PL ($E_{gap}^{PL}=1.137\pm0.001$ eV) and the value obtained from the absorbance spectrum ($E_{gap}^{Tauc}=1.16\pm0.02$ eV) is known as *Stokes Shift* and, in first approximation, can be explained using the Frank-Condon principle [37] but it is also modulated by strain [38], impurities [39, 40] and other factors. We remark that a deeper understanding of this phenomenon in $MoSe_2$ is beyond the scope of this article, here we just point out that our IR laser energy well matches the indirect band-gap width.

A. Raman spectra as a function of excitation energy: experiment and theory

2H-$MoSe_2$ belongs to the space-group symmetry D_{6h}^4 and it has 12 modes of lattice vibrations at the center of the First Brillouin Zone (FBZ) [26], namely

$$\Gamma=A_{1g}+2A_{2u}+B_{1u}+2B_{2g}+E_{1g}+2E_{1u}+2E_{2g}+E_{2u} \quad (1)$$

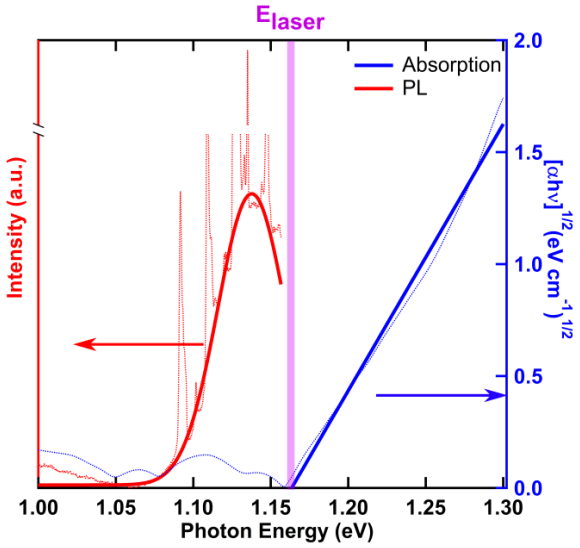

FIG. 1. Room Temperature PL (red curve) obtained fitting the background of Raman spectrum $MoSe_2$ crystal (dotted red curve). The extrapolated gap is $E_{gap}^{PL}=1.137\pm0.001$ eV. Tauc procedure (blue curve) from absorption experiment (dotted blue curve). The extrapolated gap is $E_{gap}^{Tauc}=1.16\pm0.02$ eV. We have highlighted our 1.16 eV laser energy E_{laser}.

where E_{1g}, A_{1g}, E_{2g}^1 and E_{2g}^2 are the Raman-active modes. Figure 2a shows the Raman spectra obtained at three different excitation energies. We identify three of the four first order peaks (E_{1g} at 170 cm^{-1}, A_{1g} at 243.5 cm^{-1} and E_{2g}^1 at 285 cm^{-1}). The E_{2g}^2 is at 32 cm^{-1} and below the spectral range of our FT-Raman setup. It is worth noticing that the E_{1g} mode is usually forbidden in back-scattering geometry, but it is visible at 2.33 eV probably because the laser excitation energy approaches the energy of the C-exciton (about 2.6 eV) [27, 28].

We can also identify four strongly structured Raman modes, labelled as D, S_1, S_2 and S_3 in Figure 2a, that cannot be ascribed to first order Raman scattering peaks. One can note that these modes are strongly enhanced in the spectrum taken at 1.16 eV, which is a signature of resonance processes (Figure 2b). Moreover, by looking at the S_3 mode (see Figure 3a) one can note that the overall lineshape is modified.

We first verify whether these are second order Raman modes. A Stokes second-order Raman process is related to the creation of two phonons or to the creation of one phonon and the destruction of another [41]. The resulting Raman shift will be $\hbar(\omega_1\pm\omega_2)$, where $\hbar\omega_{1,2}$ indicates the energy of the phonons and the sign is associated to creation and destruction of the phonon. One should recall that in a two-phonon process, the momentum conservation is achieved by imposing that the two phonons have opposite momentum and therefore no scattering with defects is required. Thus phonons in the entire FBZ are observable with Raman spectroscopy as long as the momentum is conserved and the non-resonant second-order Raman spectra map the two-phonon density of states, as shown for example in diamond [42].

We calculate the phonon dispersion (Figure 3b) and the

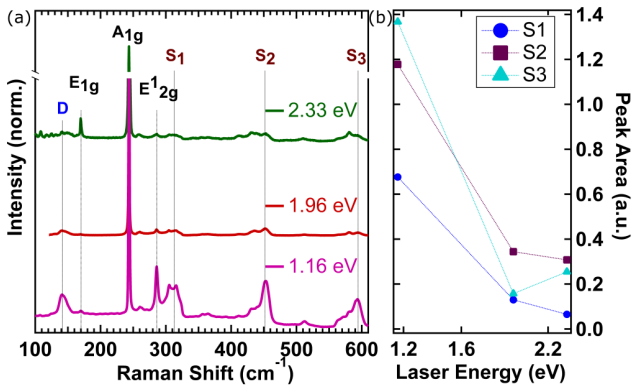

FIG. 2. (a) Spectra of $MoSe_2$ bulk taken at infrared (1.16 eV) and visible (1.96 and 2.33 eV) energies. We can observe the presence of the first order Raman peaks (labelled in black) and high order modes due to difference (labelled in blue) or summation (labelled in red) processes (see main text for their definition). The high order Raman peaks in the spectrum taken at 1.16 eV are strongly enhanced. The E_{1g} peak becomes visible as the excitation energy approaches the energy of the C-exciton (2.6 eV). All the spectra are normalized at the intensity of the A_{1g} mode and vertically shifted for sake of clarity. (b) Integrated Area of the S- Raman features, normalized to the Area of the A_{1g} peak for the different laser energies used. One can clearly see the intensity enhancement of the S- modes with respect to first-order Raman peaks.

2ph-DOS (see methods), in order to assign the phonon branches that could be involved in two-phonon scattering processes. We compare the spectrum taken with 2.33 eV photon energy with the 2ph-DOS integrated over the entire FBZ. Even without considering the matrix elements for electron-phonon and electron-light interaction, we find a striking similarity for both the energy position and the line shape between the theoretical calculations and the experimental S_3 features (see Figure 3a upper curves). This excellent lineshape agreement strongly suggests that at least the S_3 mode is due to two-phonon processes only and that using an excitation energy of 2.33 eV we do not select resonantly phonons with a specific momentum but phonon from the entire FBZ contribute equally. Therefore, we assign the S_3 mode to the sum of two phonons with opposite momenta from the B_{2g}, A_{2u}, E_{2g} and E_{1u} optical phononic branches (see Figure 3b). The second-order S_3 mode in Figure 3a, taken at 1.16 eV, shows a different lineshape. This demonstrates that there are resonant processes occurring and that not all the regions in the FBZ contribute equally in the Raman cross section. Hence, we ascribe the enhancement and the modification in the lineshape of these high-order modes obtained at 1.16 eV excitation energy to the processes resonant with the indirect band gap, as was seen previously in Si and GaP [43]. Our DFT calculations (Figure 3c) confirm that the maximum of the valence band is located at $\mathbf{\Gamma}$, while the minimum of the conduction band lies on a point, which we will call $\mathbf{T}$, which is $\mathbf{T} = \frac{t}{3}\mathbf{b_1} + \frac{t}{3}\mathbf{b_2}$ being t=0.55, $\mathbf{b_1}$ and $\mathbf{b_2}$ the reciprocal lattice vectors, and it is situated along the $\mathbf{\Gamma}$-$\mathbf{K}$ line, in accordance with previous works [21, 32, 44]. We can thus depict the resonant process as the following: an electron from the top of the valence band is excited and then scattered by a phonon with a wavevector $\mathbf{q^*} \sim \mathbf{T}$ which allows the transition to the conduction band minimum. Then, a second phonon with opposite wavevector $\mathbf{-q^*}$ brings the electron to the starting point of the FBZ and then it can relax radiatively emitting a photon (see Figure 3c). The above description can be summarized with the vanishing of the second denominator in the following expression for the intensity of the Raman process [43]:

$$I \propto \left| \sum_{\mathbf{k}} \frac{\langle v|\mathbf{P}|c\rangle \left\langle c \left| H_{ep}^{(1)} \right| c' \right\rangle \left\langle c' \left| H_{ep}^{(1)} \right| c \right\rangle \langle c|\mathbf{P}|v\rangle}{[E_g^D(\mathbf{k}) - \hbar\omega_L][E_g^{ID}(\mathbf{k}+\mathbf{q^*}) + \hbar\omega_\mu(\mathbf{q^*}) - \hbar\omega_L][E_g^D(\mathbf{k}) + \hbar\omega_\mu(\mathbf{q^*}) + \hbar\omega_\nu(\mathbf{-q^*}) - \hbar\omega_L]} \right|^2 \quad (2)$$

where the summation runs over the FBZ wavevectors, $\hbar\omega_L$ is the laser energy, $\langle v|\mathbf{P}|c\rangle$ is the momentum matrix-element between the conduction band minimum and the valence band maximum at the $\mathbf{\Gamma}$ point, separated by an energy of $E_g^D(\mathbf{k})$ and H_{ep}^1 is the electron-phonon Hamiltonian connecting the two states at $\mathbf{k}$ and $\mathbf{k}$+$\mathbf{q^*}$, separated by the energy of the indirect band-gap $E_g^{ID}(\mathbf{k}+\mathbf{q^*})$, μ and ν being the phonon branches. As it can be seen from the formula above, the Raman processes are strongly enhanced if they involve phonons with opposite momenta $\mathbf{q^*}$ and the denominator vanishes, i.e. $[E_g^{ID}(\mathbf{k}+\mathbf{q^*}) + \hbar\omega_p(\mathbf{q^*}) - \hbar\omega_L]$=0. We remark that there are other possible resonant scattering pathways that include scattering with one electron and one hole (or with two holes). Since we assume constant matrix elements these processes are all equivalent.

In order to qualitatively understand which phonons contribute to the resonance process, we restrict the sum for $DOS_{2\omega}(\varepsilon)$ to a small neighborhood of $\mathbf{q^*}$ and compare the result with the spectrum taken at IR excitation energy (Figure 3b lower curves). As it can be easily seen, by restricting the calculation of the 2ph-DOS at the particular wavevector $\mathbf{q^*}$, the spectral weight of the modes strongly changes, obtaining a qualitative agreement with the experimental spectrum at 1.16 eV. The 2ph-DOS does not match exactly the spectrum, since a complete knowledge of the matrix elements in eq.(2) would be needed, but this would fall beyond the scope of this paper. The qualitative agreement between calculation and experimental spectrum at 1.16 eV is a clear indication that the S_3 modes mostly originate from the depicted process. We note that a slight horizontal shift, around 5 cm^{-1}, was necessary to

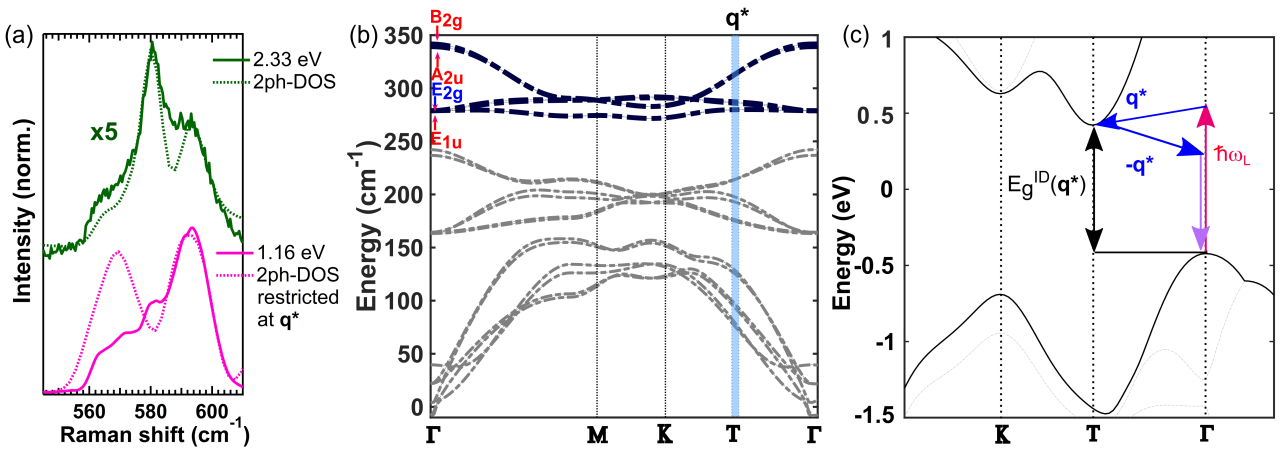

FIG. 3. (a) Raman spectra of S_3 modes compared with the 2ph-DOS. Besides the enhancement of the Raman scattering by using near-infrared excitation, the lineshape of the peaks varies by changing the excitation laser energy revealing a resonant process. The spectra are normalized to the intensity of the A_{1g} mode. (b) Phonon dispersion of bulk $MoSe_2$ restricted to the FBZ along the **Γ**-**M**-**K**-**Γ** line. The **T** point, i.e. the minimum of the conduction band, is highlighted, together with the phonon wavevector which allows the indirect electronic transition. The S_3 feature is then obtained as the direct sum of phonon branches highlighted in black, its energy being hence the sum of the energy of the two branches restricted to a neighbourhood of **T**. In red are denoted the IR active modes, in blue those Raman active. (c) Scheme of the resonant process described in this work: two phonons with opposite momenta can allow the indirect transition making the Raman process resonant. Note that the value of the energy gap is slightly underestimated by our DFT results, which is a typical feature of these calculations [17].

match the 2ph-DOS and the experimental spectra, due to possible DFT errors. Indeed slight changes to the lattice parameters and anharmonic effects can, for instance, have different effects on phonon frequencies in different zones of the FBZ, therefore resulting in overall shifts that may even be different for the total and restricted 2ph-DOS.

In previous studies in literature [27, 28, 45–50], high-order modes assignment have been proposed, mostly linking the high-order peaks to LA modes at the M point, by following the criteria that flat phonon dispersions favor defect-assisted scattering processes. Here, by comparing our 2ph-DOS to the experimental curves, we can revise such assignment for some of the high-order modes.

The S_1 modes both for 2.33 eV (see Figure 4a) and 1.16 eV (see Figure 4b) excitation laser energy have a similar lineshape to that of the calculated 2ph-DOS. In our calculations all the possible phonon pairs whose energy summed is 310 cm^{-1} are considered (e.g., $A_{1g} + E_{2g}$ or also $B_{2g} + E_{1g}$ and so on), suggesting that several possible processes build up this peak. Notably, from the 2ph-DOS restricted at **q***, a peak around 285 cm^{-1} is evident (see Figure 4b) and could explain why we observe an intense E^1_{2g} peak, with respect to what was measured in previous works [28]. In fact, the E^1_{2g} mode was shown to be resonant with the C-exciton ($\sim$ 2.6 eV) and to disappear completely for lower excitation energies [28]. We suppose that in our measurements at 1.16 eV excitation energy, this mode is enhanced by the underlying two-phonon resonant process occurring at the same energy.

The 2ph-DOS does not reproduce the S_2 modes very well. Besides a strong shift in the absolute energy (see Supplemental Material (SM) [51], section A), there is no clear match in the line shapes: a reasonable agreement can be seen between the 2ph-DOS and the experimental spectrum at 2.33 eV,

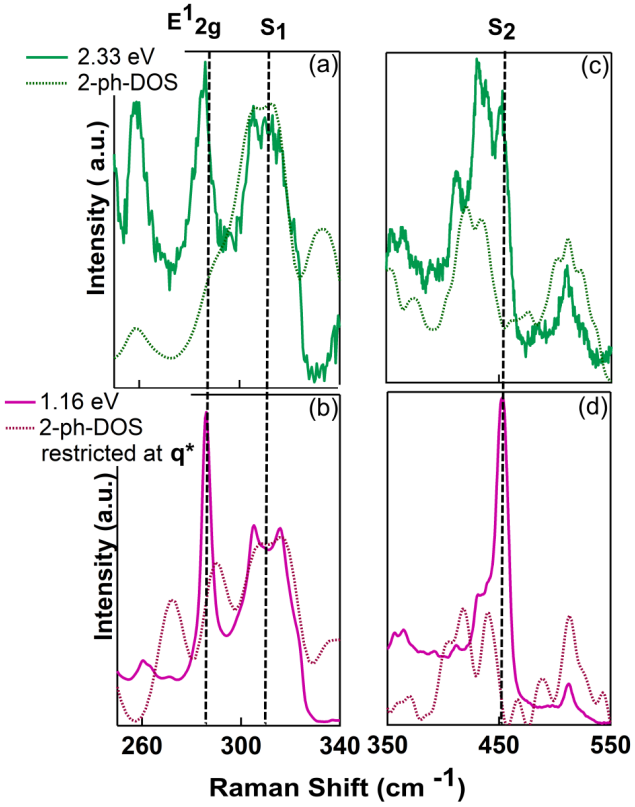

FIG. 4. (a)-(b) Comparison between the spectrum taken at 2.33 eV and the 2ph-DOS integrated over all the FBZ for different Raman Shift ranges. (c)-(d) Comparison in the same spectral ranges for the spectrum taken at 1.16 eV and the 2ph-DOS restricted at **q***.

in particular the feature around 520 cm^{-1} is very well reproduced (Figure 4c), while several differences can be found in the comparison between the restricted 2ph-DOS and the 1.16 eV Raman spectrum (Figure 4d). Furthermore, we had to add a shift of 20 cm^{-1} to the calculated DOS in order to match the data. This is an indication that, on the one hand, the S_2 modes could originate by modes with more than two phonons [27] that are not considered in our calculation or, on the other hand, that one should implement in the theory the matrix elements to better evaluate the 2ph-DOS or even that the energy of the phonon branches at the edges of the FBZ could be underestimated by our DFT calculations. We note that we could not find any experimental data of the phonon dispersion in literature, i.e. no neutron or x-ray scattering experiments, and we could not compare the DFT calculated phonon dispersion with any data. We also note that we do not observe any peaks for Raman shifts above 600 cm^{-1}, suggesting that modes with order higher than two are not strong and are below our noise level.

In the literature the D-peak has been assigned to a E_{2g}- LA difference mode, enhanced by a process resonant with the A-exciton at 1.6 eV [28]. Even if 1.16 eV excitation energy is far from the A-exciton resonance, we still observe an enhancement of the *D* mode around 148 cm^{-1}. The enhancement could originate from a process similar to the one discussed above for the S-modes. We notice also that similar resonant processes to those discussed in this paper for bulk $MoSe_2$ can be observed in monolayers for higher excitation energies. For example by measuring at 1.96 eV monolayer $MoSe_2$ we find a strong enhancement of S-like modes (see SM [51], section B), however since therein several possible scattering processes can occur, the identification of a single resonant pathway is not easily achievable.

B. Temperature dependence of Raman peaks

Further proof of the resonant origin of our S- modes could be provided with temperature dependent measurements. Indeed, it was recently shown that the indirect band gap of bulk $MoSe_2$ increases of about 100 meV by lowering the temperature [52]. We thus aim at further demonstrate the resonant origin of the S modes by driving the sample out of resonance with external temperature. In Figure 5a, we report the Raman spectra collected with 1.16 eV excitation energy between 15 K and 450 K. We see that the dominant effect of lowering the temperature is the strong reduction of the intensity of the S- and D- modes. In particular, the spectral feature *D* completely disappears at 15K, while all the other second order modes are only reduced as the temperature is lowered. Figure 5b shows the PL emission between 150 K and 450 K. We note that the data show an increase of the PL intensity and a red-shift of the correspondent band center with temperature, suggesting that in this temperature range the indirect electronic transition can be accomplished with the infrared laser energy used, this leads to the vanishing of the second denominator in eq. (2), meaning that the resonance condition is still fulfilled. What we can notice is that a minor peak at 360 cm^{-1} Raman Shift

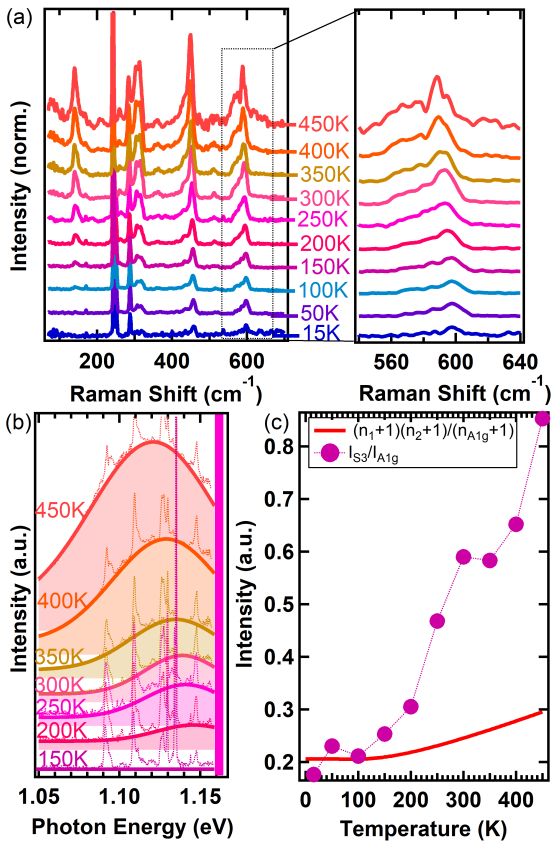

FIG. 5. (a) Temperature dependent Raman spectra of $MoSe_2$ taken at 1.16 eV plotted between 100-700 cm^{-1} and a zoom of the S_3 modes. The PL background has been subtracted to the spectra that are then normalized to the A_{1g} peak. Spectra have been offsetted for sake of clarity. (b) PL peak as extracted from Raman measurements for several temperatures indicated in figure. We observe a PL emission between 200 K and 450 K suggesting that in this temperature range we are able to reach the conduction band minimum through an indirect electronic transition, hence the resonance condition is fulfilled for the second-order Raman process described above. The vertical line represents the laser energy. (c) Comparison between the thermal occupancy given by the BE statistics and the ratio of the S_3 modes and the A_{1g} peak. We used the values $\hbar\omega_1$=310 cm^{-1} and $\hbar\omega_2$=286 cm^{-1}, as explained in the main text. The BE curve has been multiplied for a constant so to match the values of the experimental points at low temperature (i.e. to the average of the I_{S3}/I_{A1g} value of the three points below 100 K where there is no PL peak, hence no resonance condition).

gains spectral weight by increasing the temperature above 350 K and that the lineshape of S_1 and S_3 modes are modified. We can interpret this as a result of the reduction of the indirect bandgap, that thus allows for extra scattering pathways in $MoSe_2$. Indeed, only by means of thermal occupation we would not expect a modification of the lineshape.

First of all we consider the temperature dependence of the Raman intensities arising from the Bose-Einstein (BE) statistical occupation. A Stokes process, with an energy shift of $\hbar\omega_1$, has a temperature dependence of [n(ω_1,T)+1],

where n(ω_1,T)=($e^{\hbar\omega_1/k_BT}-1$)$^{-1}$ is the BE factor, T being the temperature of the crystal and k_B the Boltzmann constant. For a two-phonon process, we must consider the product [n(ω_1,T)+1][n(ω_2,T)+1], where $\hbar\omega_1$ and $\hbar\omega_2$ are the energies of the two phonons involved [41, 53]. At each temperature, a fitting procedure has been applied to A_{1g} and higher order modes using a multi-gaussian plus a linear function baseline (see SM [51], section C, for the fit procedure). We divide the intensity obtained from the fit of the higher-order modes to the corresponding intensity of the A_{1g} peak and we compare the results with the BE ratio [n(ω_1,T)+1][n(ω_2,T)+1]/[n($\omega_{A_{1g}}$,T)+1].

Figure 5c shows the temperature dependence of the BE statistics for a two-phonon process and the experimental intensity ratios for the S_3 mode (see SM [51], section D for more details about the BE trend). We used the values $\hbar\omega_1$=310 cm^{-1} and $\hbar\omega_2$=286 cm^{-1} for estimating the theoretical trend. These are intended to be only qualitative values extracted from the phonon dispersion around **T** for the high energy optical phonon branches (Figure 3b) with the constrain that $\hbar\omega_1$+$\hbar\omega_2$ should be equal to 596 cm^{-1}, the central energy of the most intense S_3 peak. Our intent was not to assign unequivocally the phonons involved but just to show that the experimental trend and the thermal one differs strongly in the measured temperature range. In Figure S4 of the Supporting Materials we plot the ratio (n_1 + 1)(n_2 + 1)/(n_{A1g}+1) for different energy values of the two phonon involved, always with the condition that $\hbar\omega_1$+$\hbar\omega_2$=596 cm^{-1}. The curves are barely distinguishable, meaning that the particular values used for the BE statistics, under the aforementioned conditions, do not affect the analysis.

The *D* feature vanishes at low temperature, as expected by the temperature-dependence of the BE ratio for phonons originating from a difference of two modes (see SM, section D). In fact, at low temperatures there are no phonons to be taken from the system or, in other words, the system cannot be cooled by phonon absorption.

The hampering of the S- Raman modes cannot be described with the reduction of the phonon occupancy only but also with the thermally-driven increase of the band gap that drives our excitation energy out-of-resonance (see Figure 5b for the S3-mode and SM, section D for the other modes). We note that we neglect possible contribution of anharmonic effects in reducing the Raman peak intensity.

III. CONCLUSIONS

In conclusion, we have investigated Raman spectra of bulk $MoSe_2$ crystals using visible (1.96 and 2.33 eV) and near-infrared (1.16 eV) excitation energies. In the latter case, we have found a significant increase in the intensity of second-order Raman modes. We have attributed this enhancement to a Raman process resonant with the indirect band gap of the crystal. We have compared the second-order Raman spectra with the two-phonon density of states calculated using a DFT approach. We have found good agreement between the Raman spectra measured with 2.33 eV excitation energy and the two-phonon density of states integrated over the entire FBZ. This demonstrates that i) most of the high order features can be ascribed to two-phonon resonances and that ii) at this photon energy the second-order Raman spectrum is not resonant with any specific indirect electronic transition with momentum away from zero. Differently, by using near-infrared excitation energy, the two-phonon Raman spectrum shows a qualitative agreement with the two-phonon density of states restricted to **q***, i.e. the wavevector of the indirect electronic transition, further indicating that this process is resonant with the $MoSe_2$ indirect band gap. To further corroborate this result, we have measured Raman spectra as a function of the sample temperature. By comparing the intensity variation of the Raman modes with the thermal statistic of phononic occupation, we have ascribed the peak intensity decrease to a thermally-driven out-of-resonance condition due to the increase of the band-gap energy at low temperatures.

Understanding Raman scattering is of primary importance for different applications, such as growth quality control or individuation of $MoSe_2$ minerals, and gives a precious insight on the phonon dispersion and its coupling with electrons at the bottom of the conduction band [54]. This study broadens the understanding of the resonance Raman spectrum in $MoSe_2$ and shows that Raman scattering with near-infrared excitation energy is a precious complementary tool for the study of van der Waals semiconductors. In perspective, we envision that one could make use of a near-infrared tunable lasers to probe the phonon dispersion away from zone center by means of resonance Raman in small-gap semiconductors.

ACKNOWLEDGMENTS

The authors thank Lorenzo Graziotto and Francesco Mauri for helpful and friendly discussions. We acknowledge the European Union's Horizon 2020 research and innovation program under grant agreements no. 881603-Graphene Core3. We acknowledge support from the PRIN2017 grant number 2017Z8TS5B. We acknowledge that the results of this research have been achieved using the DECI resource Mahti CSC based in Finland at https://research.csc.fi/-/mahti with support from the PRACE aisbl. We also aknowledge PRACE for awarding us access to Juliot-Curie at TGCC, France.

[1] M. Cardona and R. Merlin, Light scattering in solids ix, Light Scattering in Solid IX , 1 (2006).

[2] P. Brüesch, *Phonons: Theory and Experiments II: Experiments and Interpretation of Experimental Results*, Vol. 65 (Springer Science & Business Media, 2012).

[3] B. R. Carvalho and M. A. Pimenta, Resonance raman spectroscopy in semiconducting transition-metal dichalcogenides: basic properties and perspectives, 2D Materials **7**, 042001 (2020).

[4] J.-U. Lee and H. Cheong, Resonance raman effects in transition metal dichalcogenides, Journal of Raman Spectroscopy **49**, 66 (2018).

[5] M. Placidi, M. Dimitrievska, V. Izquierdo-Roca, X. Fontané, A. Castellanos-Gomez, A. Pérez-Tomás, N. Mestres, M. Espindola-Rodriguez, S. López-Marino, M. Neuschitzer, *et al.*, Multiwavelength excitation raman scattering analysis of bulk and two-dimensional MoS2: vibrational properties of atomically thin MoS2 layers, 2D Materials **2**, 035006 (2015).

[6] L. Malard, M. A. Pimenta, G. Dresselhaus, and M. Dresselhaus, Raman spectroscopy in graphene, Physics Reports **473**, 51 (2009).

[7] A. C. Ferrari, J. C. Meyer, V. Scardaci, C. Casiraghi, M. Lazzeri, F. Mauri, S. Piscanec, D. Jiang, K. S. Novoselov, S. Roth, *et al.*, Raman spectrum of graphene and graphene layers, Physical Review Letters **97**, 187401 (2006).

[8] S. Caramazza, A. Collina, E. Stellino, F. Ripanti, P. Dore, and P. Postorino, First-and second-order raman scattering from MoTe2 single crystal, The European Physical Journal B **91**, 1 (2018).

[9] R. Saito, Y. Tatsumi, S. Huang, X. Ling, and M. Dresselhaus, Raman spectroscopy of transition metal dichalcogenides, Journal of Physics: Condensed Matter **28**, 353002 (2016).

[10] A. Eckmann, A. Felten, A. Mishchenko, L. Britnell, R. Krupke, K. S. Novoselov, and C. Casiraghi, Probing the nature of defects in graphene by raman spectroscopy, Nano Letters **12**, 3925 (2012).

[11] Z. Wu and Z. Ni, Spectroscopic investigation of defects in two-dimensional materials, Nanophotonics **6**, 1219 (2017).

[12] C. Cong, T. Yu, K. Sato, J. Shang, R. Saito, G. F. Dresselhaus, and M. S. Dresselhaus, Raman characterization of aba-and abc-stacked trilayer graphene, ACS Nano **5**, 8760 (2011).

[13] M. O'Brien, N. McEvoy, D. Hanlon, T. Hallam, J. N. Coleman, and G. S. Duesberg, Mapping of low-frequency raman modes in cvd-grown transition metal dichalcogenides: layer number, stacking orientation and resonant effects, Scientific reports **6**, 1 (2016).

[14] T. Mueller and E. Malic, Exciton physics and device application of two-dimensional transition metal dichalcogenide semiconductors, npj 2D Materials and Applications **2**, 1 (2018).

[15] Q. H. Wang, K. Kalantar-Zadeh, A. Kis, J. N. Coleman, and M. S. Strano, Electronics and optoelectronics of two-dimensional transition metal dichalcogenides, Nature Nanotechnology **7**, 699 (2012).

[16] P. Tonndorf, R. Schmidt, P. Böttger, X. Zhang, J. Börner, A. Liebig, M. Albrecht, C. Kloc, O. Gordan, D. R. Zahn, *et al.*, Photoluminescence emission and raman response of monolayer MoS2, MoSe2, and WSe2, Optics Express **21**, 4908 (2013).

[17] S. Tongay, J. Zhou, C. Ataca, K. Lo, T. S. Matthews, J. Li, J. C. Grossman, and J. Wu, Thermally driven crossover from indirect toward direct bandgap in 2d semiconductors: MoSe2 versus MoS2, Nano letters **12**, 5576 (2012).

[18] T. Venanzi, M. Selig, S. Winnerl, A. Pashkin, A. Knorr, M. Helm, and H. Schneider, Terahertz-induced energy transfer from hot carriers to trions in a MoSe2 monolayer, ACS Photonics **8**, 2931–2939 (2021).

[19] A. Eftekhari, Molybdenum diselenide (MoSe2) for energy storage, catalysis, and optoelectronics, Applied Materials Today **8**, 1 (2017).

[20] P. J. Ko, A. Abderrahmane, N.-H. Kim, and A. Sandhu, High-performance near-infrared photodetector based on nano-layered MoSe2, Semiconductor Science and Technology **32**, 065015 (2017).

[21] S. Kumar and U. Schwingenschlogl, Thermoelectric response of bulk and monolayer MoSe2 and WSe2, Chemistry of Materials **27**, 1278 (2015).

[22] M. Bernardi, M. Palummo, and J. C. Grossman, Extraordinary sunlight absorption and one nanometer thick photovoltaics using two-dimensional monolayer materials, Nano letters **13**, 3664 (2013).

[23] S. Poncé, F. Macheda, E. R. Margine, N. Marzari, N. Bonini, and F. Giustino, First-principles predictions of hall and drift mobilities in semiconductors, Physical Review Research **3**, 043022 (2021).

[24] F. Macheda, S. Poncé, F. Giustino, and N. Bonini, Theory and computation of hall scattering factor in graphene, Nano Letters **20**, 8861 (2020).

[25] F. Macheda, P. Barone, and F. Mauri, Frohlich electron-phonon interaction and LO-TO splitting in doped semiconductors, arXiv preprint arXiv:2202.02835 (2022).

[26] T. Sekine, M. Izumi, T. Nakashizu, K. Uchinokura, and E. Matsuura, Raman scattering and infrared reflectance in 2h-MoSe2, Journal of the Physical Society of Japan **49**, 1069 (1980).

[27] P. Soubelet, A. E. Bruchhausen, A. Fainstein, K. Nogajewski, and C. Faugeras, Resonance effects in the raman scattering of monolayer and few-layer MoSe2, Physical Review B **93**, 155407 (2016).

[28] D. Nam, J.-U. Lee, and H. Cheong, Excitation energy dependent raman spectrum of MoSe2, Scientific reports **5**, 1 (2015).

[29] K. Kim, J.-U. Lee, D. Nam, and H. Cheong, Davydov splitting and excitonic resonance effects in raman spectra of few-layer MoSe2, ACS nano **10**, 8113 (2016).

[30] A. Mooradian and G. Wright, First order Raman effect in III–V compounds, Solid State Communications **4**, 431 (1966).

[31] S. Grimme, J. Antony, S. Ehrlich, and H. Krieg, A consistent and accurate ab initio parametrization of density functional dispersion correction (DFT-D) for the 94 elements H-Pu, The Journal of Chemical Physics **132**, 154104 (2010).

[32] H.-g. Kim and H. J. Choi, Thickness dependence of work function, ionization energy, and electron affinity of Mo and W dichalcogenides from DFT and GW calculations, Physical Review B **103**, 085404 (2021).

[33] S. Baroni, S. De Gironcoli, A. Dal Corso, and P. Giannozzi, Phonons and related crystal properties from density-functional perturbation theory, Reviews of Modern Physics **73**, 515 (2001).

[34] P. Giannozzi, S. Baroni, N. Bonini, M. Calandra, R. Car, C. Cavazzoni, D. Ceresoli, G. L. Chiarotti, M. Cococcioni, I. Dabo, *et al.*, QUANTUM ESPRESSO: a modular and open-source software project for quantum simulations of materials, Journal of Physics: Condensed Matter **21**, 395502 (2009).

[35] A. Zanatta, Revisiting the optical bandgap of semiconductors and the proposal of a unified methodology to its determination,

Scientific Reports **9**, 1 (2019).

[36] P. Makuła, M. Pacia, and W. Macyk, How to correctly determine the band gap energy of modified semiconductor photocatalysts based on uv–vis spectra, J. Phys. Chem. Lett **9**, 6814–6817 (2018).

[37] I. Pelant and J. Valenta, *Luminescence spectroscopy of semiconductors* (OUP Oxford, 2012).

[38] I. Niehues, P. Marauhn, T. Deilmann, D. Wigger, R. Schmidt, A. Arora, S. M. de Vasconcellos, M. Rohlfing, and R. Bratschitsch, Strain tuning of the stokes shift in atomically thin semiconductors, Nanoscale **12**, 20786 (2020).

[39] Y. Kanemitsu and S. Okamoto, Phonon structures and Stokes shift in resonantly excited luminescence of silicon nanocrystals, Physical Review B **58**, 9652 (1998).

[40] E. Martin, C. Delerue, G. Allan, and M. Lannoo, Theory of excitonic exchange splitting and optical Stokes shift in silicon nanocrystallites: Application to porous silicon, Physical Review B **50**, 18258 (1994).

[41] J. Potts, C. T. Walker, and I. R. Nair, Temperature dependence of second-order raman scattering in potassium and rubidium halides, Physical Review B **8**, 2756 (1973).

[42] W. Windl, P. Pavone, K. Karch, O. Schütt, D. Strauch, P. Giannozzi, and S. Baroni, Second-order raman spectra of diamond from ab initio phonon calculations, Physical Review B **48**, 3164 (1993).

[43] P. Klein, H. Masui, J.-J. Song, and R. Chang, Selective resonant enhancement in the two-phonon raman spectrum of Si and GaP, Solid State Communications **14**, 1163 (1974).

[44] R. Coehoorn, C. Haas, J. Dijkstra, C. J. F. Flipse, R. A. deGroot, and A. Wold, Electronic structure of MoSe2, MoS2, and WSe2. i. band-structure calculations and photoelectron spectroscopy, Physical Review B **35**, 6195 (1987).

[45] J. Chen and C. Wang, Second order raman spectrum of MoS2, Solid State Communications **14**, 857 (1974).

[46] K. Gołasa, M. Grzeszczyk, P. Leszczyński, C. Faugeras, A. Nicolet, A. Wysmołek, M. Potemski, and A. Babiński, Multiphonon resonant raman scattering in MoS2, Applied Physics Letters **104**, 092106 (2014).

[47] K. Gołasa, M. Grzeszczyk, R. Bożek, P. Leszczyński, A. Wysmołek, M. Potemski, and A. Babiński, Resonant raman scattering in MoS2—from bulk to monolayer, Solid State Communications **197**, 53 (2014).

[48] A. Stacy and D. Hodul, Raman spectra of IVB and VIB transition metal disulfides using laser energies near the absorption edges, Journal of Physics and Chemistry of Solids **46**, 405 (1985).

[49] G. L. Frey, R. Tenne, M. J. Matthews, M. S. Dresselhaus, and G. Dresselhaus, Raman and resonance raman investigation of MoS2 nanoparticles, Physical Review B **60**, 2883 (1999).

[50] B. Chakraborty, H. R. Matte, A. Sood, and C. Rao, Layer-dependent resonant raman scattering of a few layer MoS2, Journal of Raman Spectroscopy **44**, 92 (2013).

[51] See Supplemental Material at [] for more information regarding the experimental details and additional analysis.

[52] J. Kopaczek, S. Zelewski, K. Yumigeta, R. Sailus, S. Tongay, and R. Kudrawiec, Temperature Dependence of the Indirect Gap and the Direct optical Transitions at the High-Symmetry Point of the Brillouin Zone and Band Nesting in MoS2, MoSe2, MoTe2, WS2, and WSe2 crystals, The Journal of Physical Chemistry C (2022).

[53] A. A. Mitioglu, P. Plochocka, G. Deligeorgis, S. Anghel, L. Kulyuk, and D. K. Maude, Second-order resonant raman scattering in single-layer tungsten disulfide WS 2, Physical Review B **89**, 245442 (2014).

[54] F. Macheda and N. Bonini, Magnetotransport phenomena in p-doped diamond from first principles, Physical Review B **98**, 201201(R) (2018).